Frontiers in Heat and Mass Transfer

Available at www.ThermalFluidsCentral.org

EFFECTS OF BLOCKAGE LOCATIONS FOR ENHANCED HEAT TRANSFER AND FLOW VISUALIZATION IN A TESTED DUCT WITH DUAL-INCLINED BAFFLES (DIB): A CFD ANALYSIS

Amnart Boonloi[a] and Withada Jedsadaratanachai[b,*]

[a] Department of Mechanical Engineering Technology, College of Industrial Technology, King Mongkut's University of Technology North Bangkok, Bangkok 10800, Thailand
[b] Department of Mechanical Engineering, School of Engineering, King Mongkut's Institute of Technology Ladkrabang, Bangkok 10520, Thailand

ABSTRACT

Numerical analysis of fluid flow mechanism and heat transfer in a heat exchanger duct (HXD) with dual-inclined baffles (DIB) are reported. Three DIB types are examined: 1. "Type A" is located at the center of the HXD, 2. "Type B" is located on the upper-lower duct walls (as an orifice) and 3. "Type C" is a combination of the type A and B (as double orifices). The impacts of the ratio of DIB heights (b) to the square duct height (H; b/H) on increased heat transfer and friction loss are analyzed. Laminar flow (Re = 100 – 2000 based on the entry condition of the tested duct) is discussed. The simulated problems of the HXD equipped with various DIB types are analyzed by a commercial code (the finite volume method). To confirm accuracy results, the simulated domain of the HXD with the DIB is validated (optimum grid check and smooth duct validation). The simulated solutions are illustrated in terms of heat transfer and flow features. The performance assessments of the HXD with different DIB types are also presented in terms of thermal enhancement factor, Nusselt number and friction factor. It is interesting that the changed DIB position at an identical flow-blockage-ratio leads to the changed flow structure that impacts the variations of both the Nusselt number and pressure drop of the HXD. It is found that type C DIB provides the greatest thermal potentiality. The heat transfer rate of the HXD equipped with type A, B and C DIB is 1.38 – 13.93, 1.00 – 14.19 and 1.31 – 14.45 times higher than that of the smooth duct, respectively, depending on the DIB height and Reynolds number. Additionally, the best thermal enhancement factor (TEF) of 4.04 is found for the HXD with the type C DIB at $b_1/H = 0.05$ and $b_2/H = 0.15$ at Re = 2000.

Keywords: heat transfer; heat exchanger duct; vortex generator; thermal enhancement factor; vortex flow; dual-inclined baffles.

1. INTRODUCTION

Vortex generators or turbulators are devices used to augment heat transfer rate in heating/cooling systems or production processes such as chemical processes, food processes, power plants, automotive industries, etc. Development of the vortex generators is the key to thermal performance development of heat exchangers. The thermal performance improvement of the heat exchangers leads to energy saving and production cost of the production processes. An installation of the vortex generators in the heat exchangers modifies general flow and heat transfer. Longitudinal vortex flows and impinging flows are found when the vortex generators are installed in the heat exchangers. These flow structures may disturb thermal boundary layer (TBL) which causes an increase in the heat transfer coefficient and thermal efficiency. The flow structure and heat transfer characteristics change with types, placement and other parameters of vortex generators. The fluid flow and heat transfer mechanisms in various heat exchangers equipped with different vortex generators have been investigated by many researchers.

There are two configurations of ribs/baffles: inclined- and V-shaped ribs/baffles, which are used to improve heat transfer efficiency in many heating/cooling systems and heat exchanger devices. Examples of the investigations of the inclined and V-shaped ribs/baffles are as follows. Rathor and Aharwal (2020) experimentally examined the augmented heat transfer with the use of a staggered element in a rectangular duct inserted with inclined discrete ribs. They found that flow strength increased due to the increment of the turbulent intensity. They found the enhanced thermo-hydraulic performance to be around 2.06 at Reynolds number of 12,438. Sivakandhan et al. (2020) examined the enhanced thermal potentiality in a new hybrid duct of a solar air heater with

inclined ribs. The effects of relative roughness pitches, relative roughness heights and relative angles were considered. Yuan et al. (2020) reported the fluid stream and heat transfer of supercritical pressure CO_2 in pipes with discrete double inclined ribs as vortex generators. They found that the influence of the inclination angle is less significant than that of the rib height and the rib spacing. Liu et al. (2021) studied the film cooling behavior of a coolant passage with different hole locations and inclined ribs. Barik et al. (2021) reported an increase in heat transfer of a solar air heater inserted with various ribs (T-rib, left arm inclined T-rib, right arm inclined T-rib, Y-rib, concave and convex T-ribs). Their results revealed that the Nusselt number of the T-rib enhances by 191% over a range of Reynolds numbers around 5000 – 18,000. Luan and Phu (2020) presented the thermo-hydraulic correlations and the exergy assessment of a solar air heater equipped with inclined baffles. The inclination angles, 0º – 180º, of the inclined rib were compared. They concluded that the best inclination angles are around 60º – 120º. Chang et al. (2019) examined the enhanced heat transfer in a square channel heat exchanger equipped with inclined baffles and perforated slots. They concluded that the averaged Nusselt number and friction loss are around 5 – 9 times and 5 – 85 times greater than the smooth correlations of the averaged Nusselt number and friction factor, respectively. Keramet et al. (2020) studied the natural convective heat transfer in an H-shaped enclosure equipped with V-shaped baffles combined with nanofluid using a numerical method. Jiang et al. (2021) analyzed the augmented heat transfer for a liquid cold plate with mini V-shaped ribs for battery packs. They found that the Nusselt number and friction factor of the baffle with the V-shaped ribs are greater than those of the channel with straight ribs. Bahiraei et al. (2020) improved the 2nd law characteristics of flow in a square channel inserted with V-shaped ribs combined with nanofluid. The influences of rib pitches and rib heights were analyzed.

(a)

(b)

(c)

TYPE A   TYPE B   TYPE C

(d)
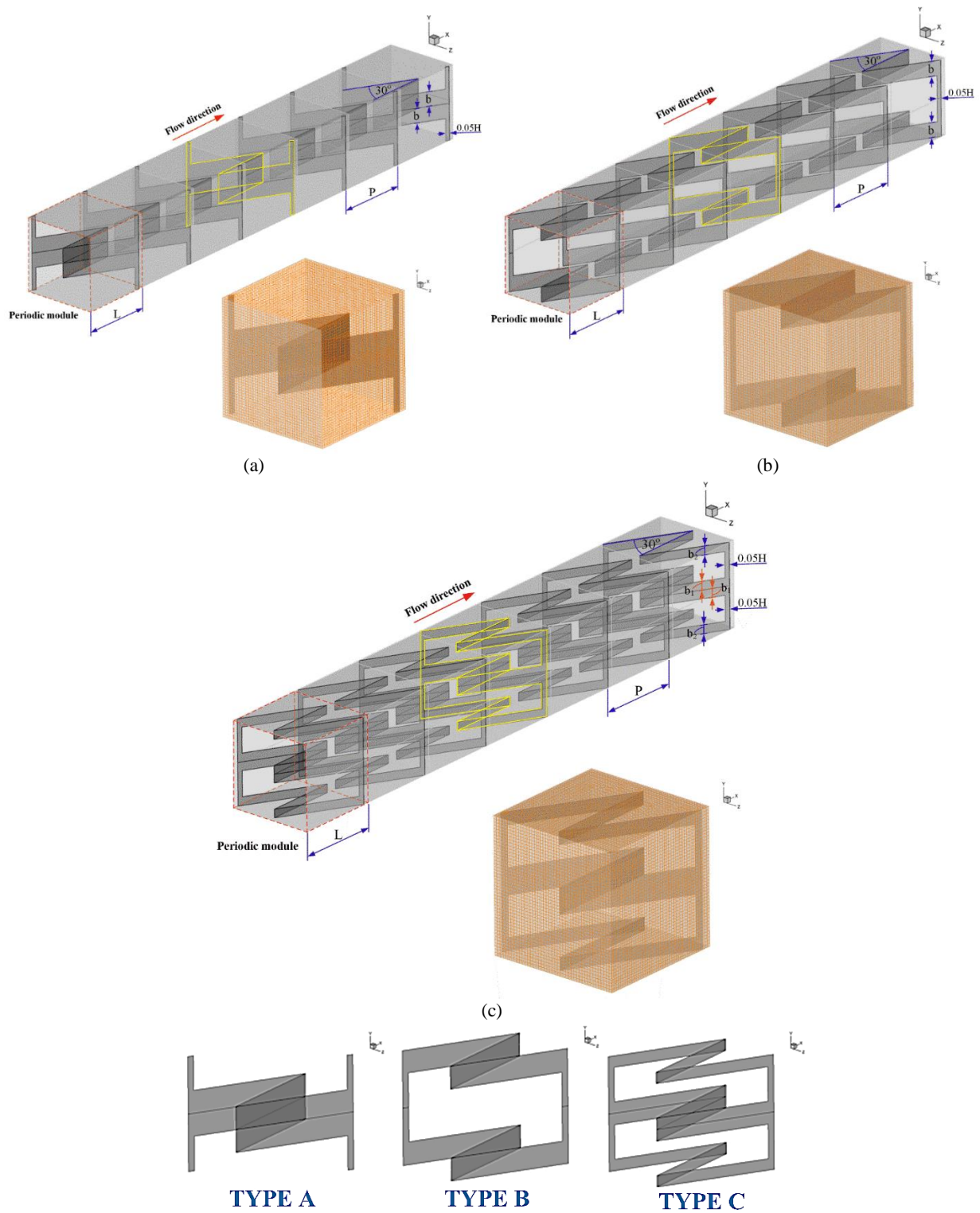
Fig. 1   (a) square channel inserted with type A DIB, (b) square channel inserted with type B DIB, (c) square channel inserted with type C DIB and (d) the DIB configurations.
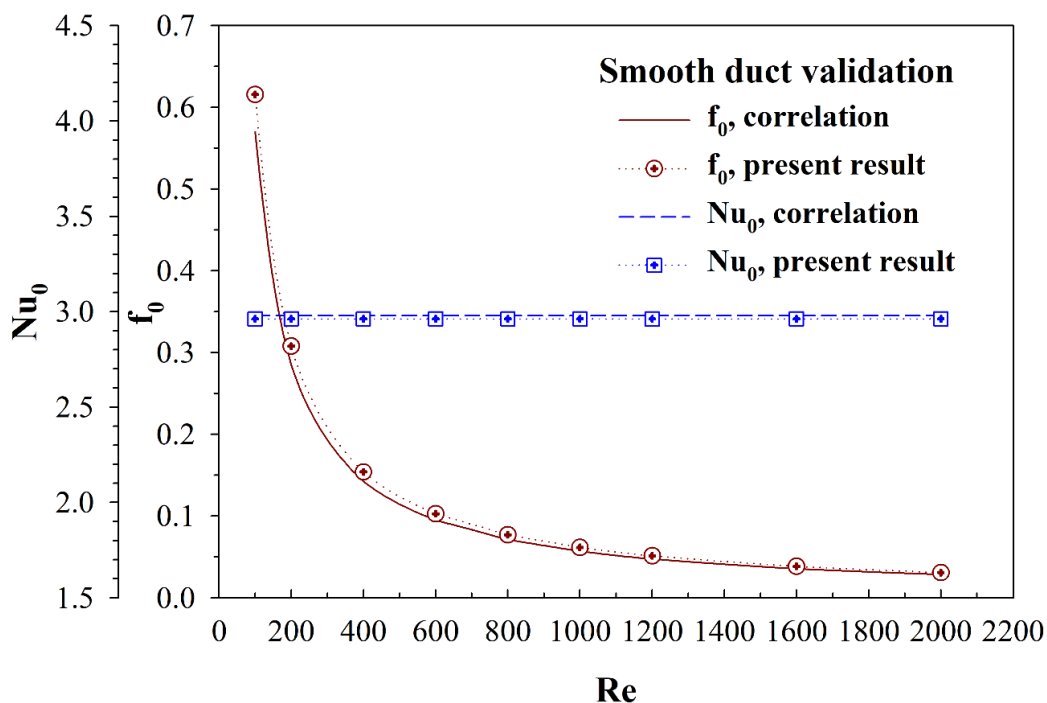
Fig. 2   Validations of the plain duct.

(a)

(b)
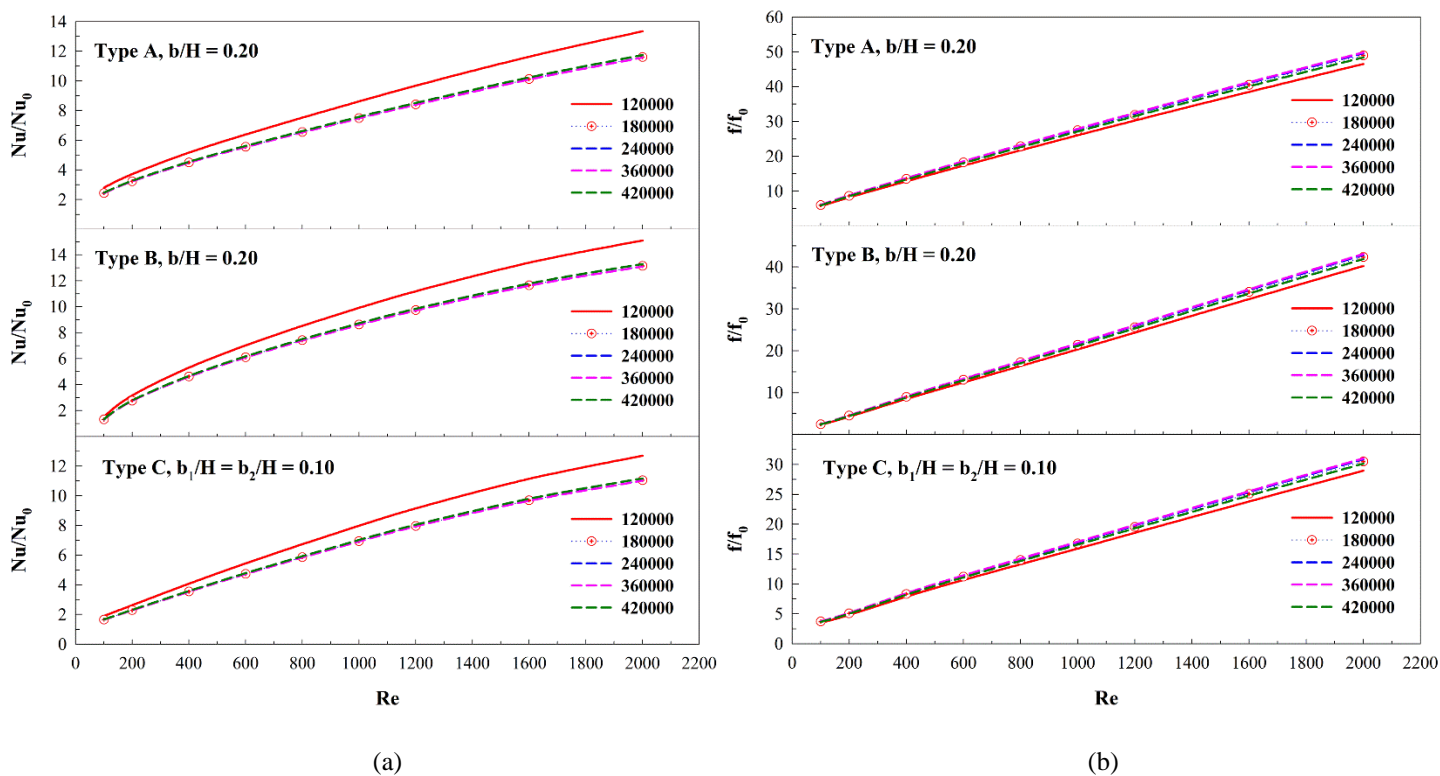
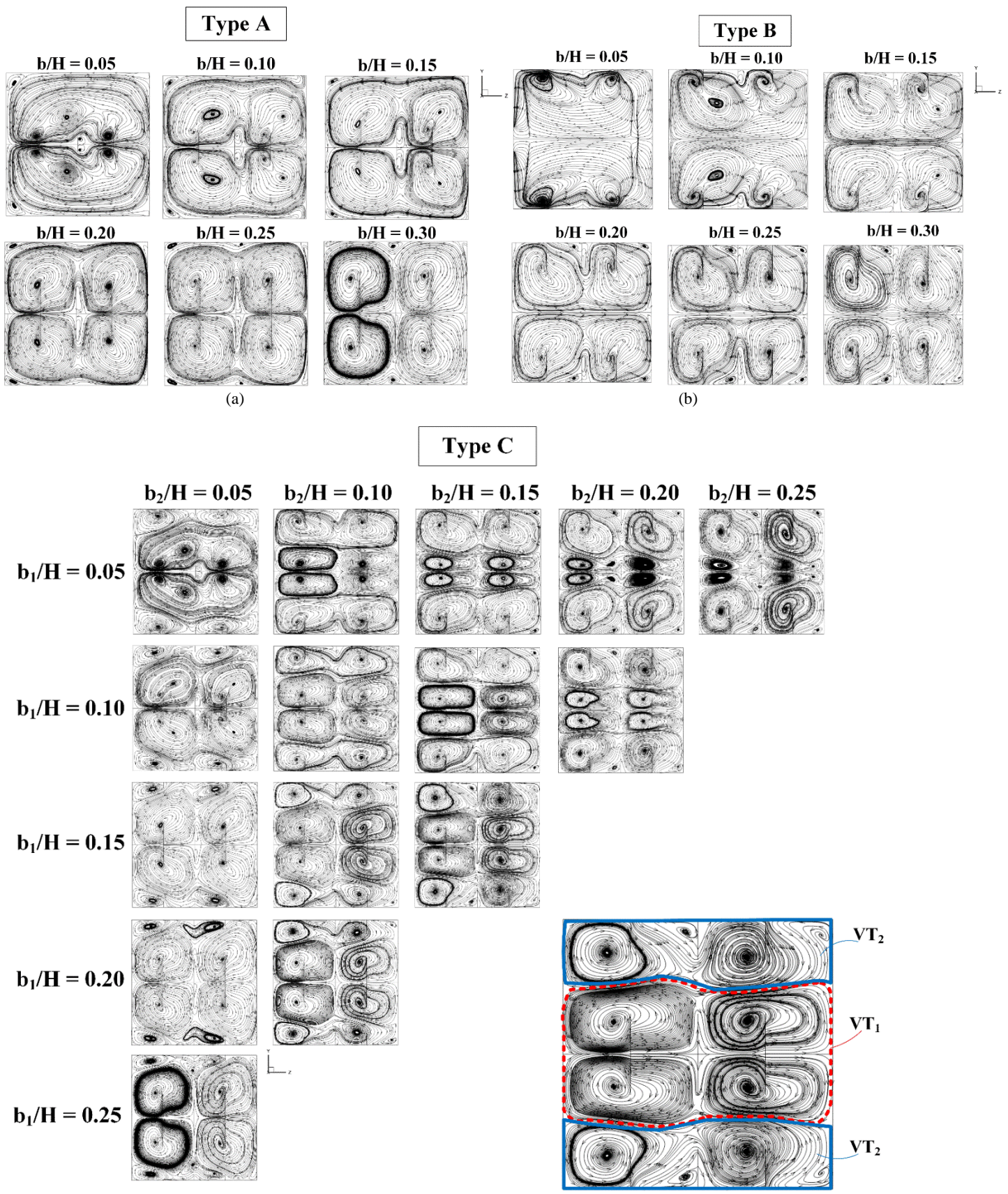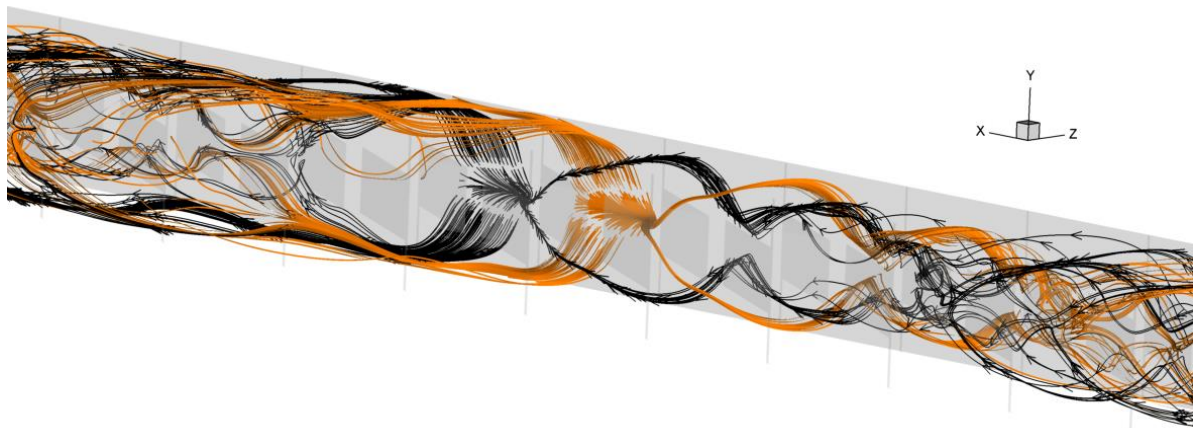**Fig. 3**   Grid independence of the HXD equipped with various DIB types for (a) Nu/Nu_0 and (b) f/f_0.
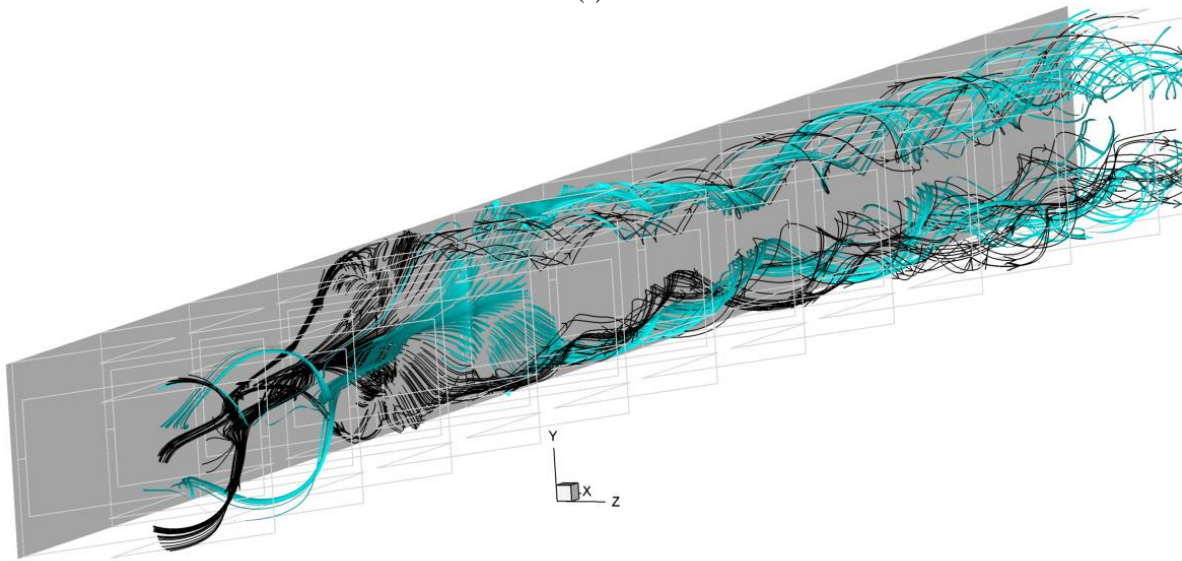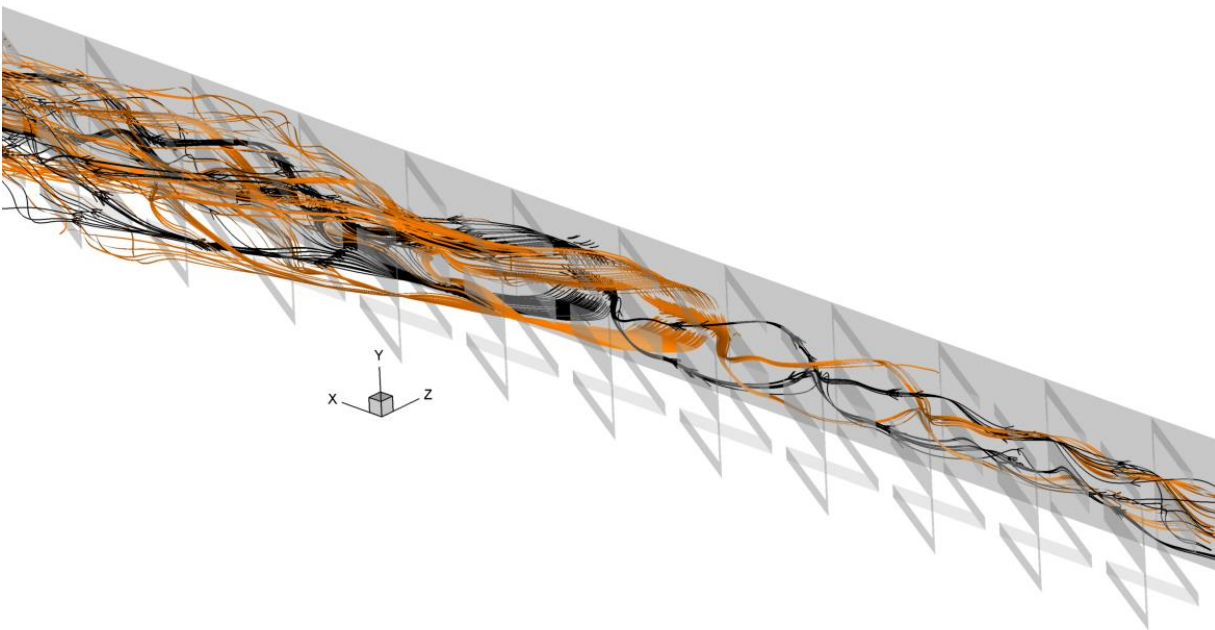
Fig. 4 Streamlines in transverse planes of the HXD equipped with various DIB types for (a) type A, (b) type and (c) type C at Re = 1000.

(a)
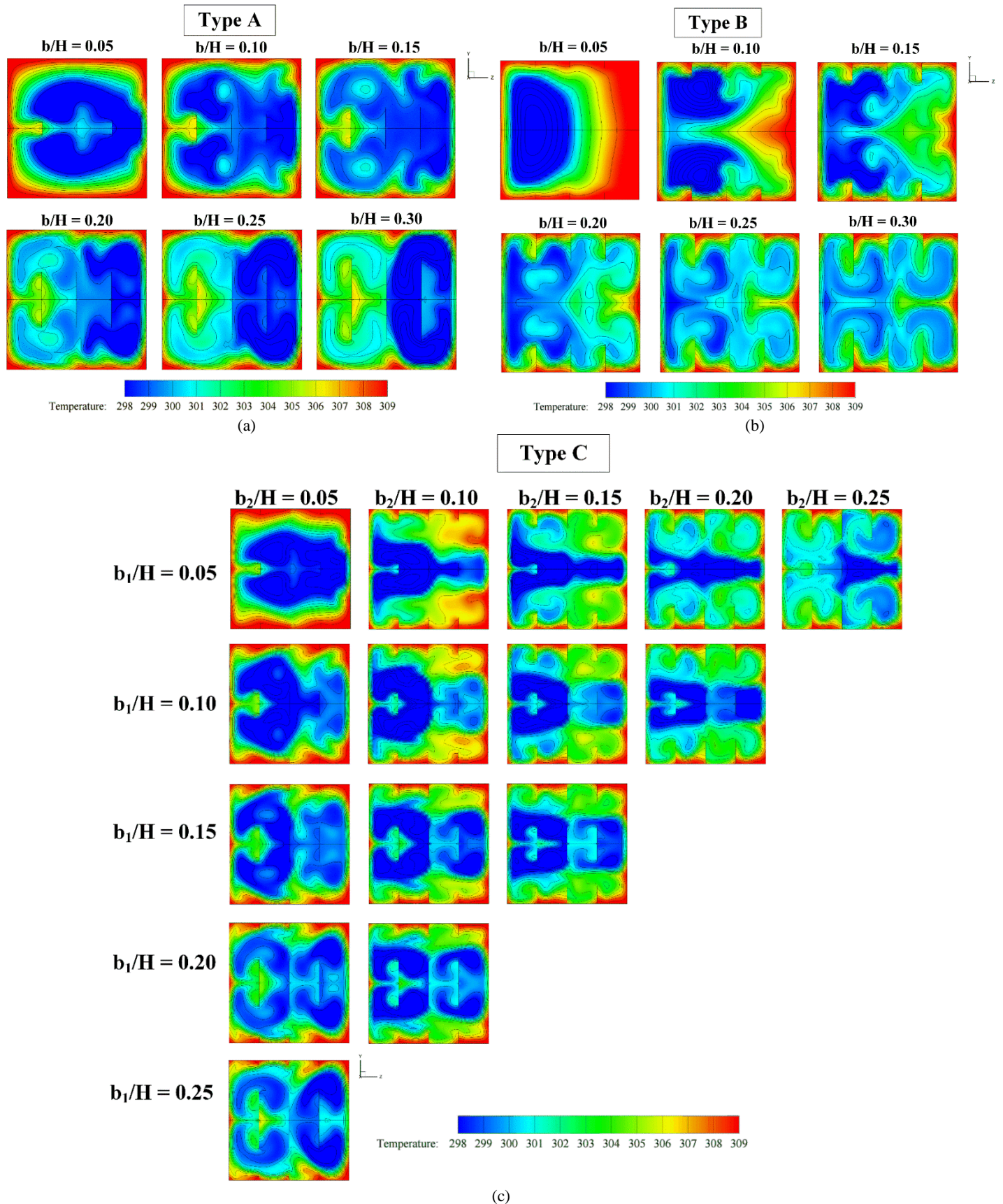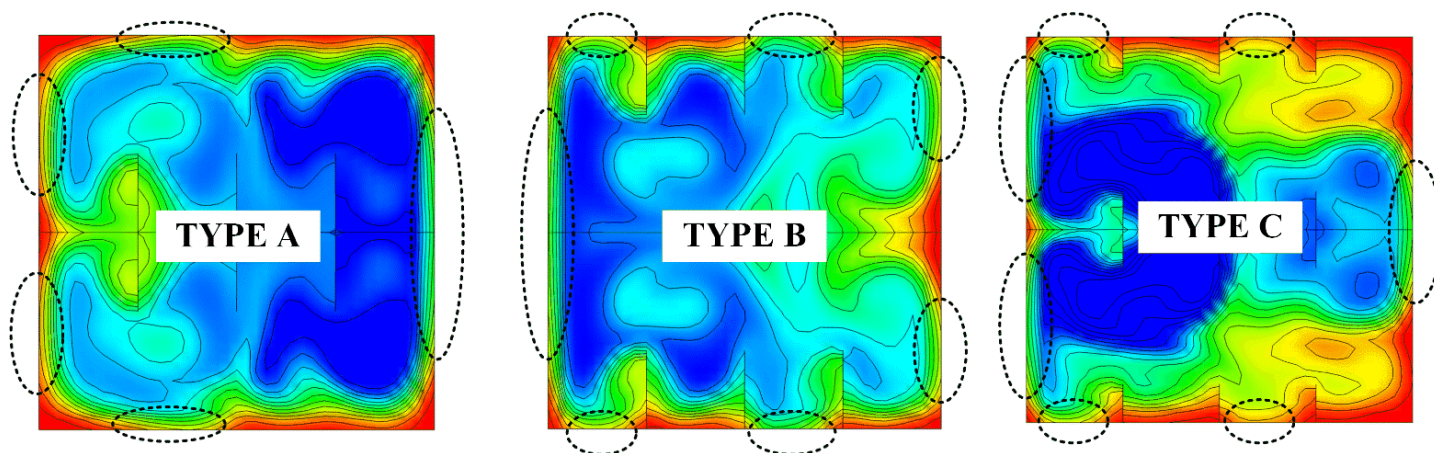

(b)

(c)

Fig. 5 Longitudinal vortex flows of the HXD equipped with various DIB types for (a) type A (b/H = 0.20), (b) type (b/H = 0.20) and (c) type C (b_1/H = b_2/H = 0.10) at Re = 1000.

Fig. 6 Fluid temperature contours in transverse planes of the HXD equipped with various DIB types for (a) type A, (b) type and (c) type C at Re = 1000.

Fig. 7 The locations of the disturbed TBL on the duct wall of the HXD with various DIB types.

They reported that the increased rib height with the declined rib distance results in lower exergy destruction and enhances the 2nd efficiency. Bahiraei et al. (2019) simulated the enhanced thermal potentiality of Cu-water nanofluid for a square channel inserted with 90° V-shaped ribs. They concluded that the augmented heat transfer is around 28.3% when the rib height is increased from 2.5 to 7.5 mm with rib spacing of 50 mm. Jin et al. (2019) numerically analyzed the augmented Nusselt number of a solar air heater with multiple V-shaped ribs. Krishnaswamy and Sivan (2021) employed continuous V and W-shaped ribs to improve thermal potentiality of gas turbine blade. They found that the V and W-shaped ribs provides the maximum Nusselt number ratio of around 3.9 and 3.8, respectively. They also reported that the greatest thermal potentiality is around 3.3 and 3.0 for the V and W-shaped ribs, respectively. Zheng et al. (2019) numerically simulated the fluid stream and thermal profile in a rectangular channel inserted with five different V-shaped slit ribs (ribs with rectangular slits, V-shaped slits, anti-V-shaped slits, broken V-shaped slits and broken anti-V-shaped slits). The numerical results revealed that the channel inserted with the broken slits provided greater thermal performance due to higher turbulent intensity. Zhao et al. (2021) selected ribs combining with delta winglet vortex generators to augment heat transfer rate of a solar air heater. The effects of different vortex generator types including 90° continuous ribs, 90° truncated ribs, 60° V-shaped continuous ribs, and 60° V-shaped truncated ribs, were compared. They indicated that the delta winglet vortex generators combined with the 60° V-shaped continuous ribs provide the greatest thermal potentiality. They also presented that the augmented heat transfer is around 39.4% when compared with the single delta winglet vortex generators. Ni et al. (2019) presented three different ribs: rectangular, ⋂-shaped and U-shaped ribs, in micro-combustors. They found that the 2nd law efficiency increased around 46 – 51% over their studied range. Srivastava et al. (2020) numerically and experimentally studied the impacts of ribs on an absorber plate in a solar air heater. The arc-shape with gaps was compared with the V-shaped with gaps. They informed that the enhanced Nusselt number was around 3.4 and 2.4 for the V-shaped and are-shaped ribs, respectively. Ameur et al. (2020) enhanced the cooling of shear-thinning fluids with the V-baffling technique. They concluded that the maximum enhanced heat transfer ratio was about 1.52. Ameur and Sahel (2019) studied the effects of some parameters on the thermo-hydraulic characteristics of a channel heat exchanger with corrugated walls. Menni et al. (2020) improved solar duct efficiency by using multiple V-baffles. Ameur (2019) investigated the effects of the baffle inclination on the flow and thermal characteristics in channel heat exchangers. Ameur (2020) found that the overall performance factor increased from 1.27 to 1.53 when the corrugation angle of the corrugated baffle was increased from 0° to 45°. Luan and Phu (2021) numerically analyzed the thermal performance and entropy generation of the baffled channel. Thao et al. (2021) performed a CFD study and Taguchi-Based optimization of a solar air heater duct baffled on a back plate. Phu et al.

(2021) found that the maximum effective efficiency of the baffled collector duct with successive ratios from 1 to 1.3 was 0.6.

As shown in the previous works, the investigations of the heat exchanger with the vortex generators can be done by both numerical and experimental studies. Insights in fluid flow and heat transfer are key to developing new designs of the vortex generators and heat exchangers. Moreover, a numerical study, compared with an experimental study, is an inexpensive approach. However, an accuracy of numerical results must be assessed. The simulated domain of a heat exchanger mounted with vortex generators must be compared with the correlation values or experimental data to confirm the credibility of the numerical model.

From the published works, a single V-shape generator produces two main counter-rotating flows with common-flow-up/down. The counter-rotating flows highly disturb the TBL only near upper-lower walls or left-right sidewalls depending on the V-tip arrangement. Therefore, in the present work, we try to produce two main co-rotating flows. It is assumed that the co-rotating flows may disturb the TBL in all sides of the heating duct. In the present research, the heat exchanger duct (HXD) equipped with the dual-inclined baffles (DIB) is considered. The effects of DIB types and DIB heights on topologies and heat transfer of laminar flow are discussed. The DIB configurations are categorized into three types: type A, B and C. The installation and maintenance of various DIB types in real heating/cooling systems are also provided.

2. THE HXD EQUIPPED WITH VARIOUS DIB TYPES

Figs. 1a, b and c present the HXD equipped with type A, B and C DIBs, respectively. The DIB can be categorized into three types: 1. Type A DIB is installed at the center of the HXD, 2. Type B DIB is installed on the upper-lower walls of the HXD and 3. Type C DIB is type A and B DIBs combined. The square duct is considered for the present research. The square duct height is equivalent to 0.05m. The hydraulic diameter of the square duct, D_h, is equal to the duct height ($D_h = H$). The periodic model length of the HXD equipped with the DIB, L, is fixed to H or L/H = 1. DIB spacing, P, is equal to H (P/H = 1). An inclination angle or flow attack angle of the DIB is 30°. The baffle thickness at the left-right sidewalls of 0.05H is set for all investigated cases. The DIB height of type A and B DIBs is represented with "b". For type C DIB, "b_1" is the DIB height at the center of the HXD, while "b_2" is the DIB height on the upper-lower walls. For type A and B DIBs, the DIB height to the duct height, b/H, is varied as follows: 0.05, 0.10, 0.15, 0.20, 0.25 and 0.30. For type C DIB, the total DIB height (b_1+b_2) is not higher than 30% of the duct height, $b_t/H \leq 0.30$. The investigated cases of type C DIB are listed in Table 1. The flow direction in positive x-axis (+x) is considered for all studied cases.
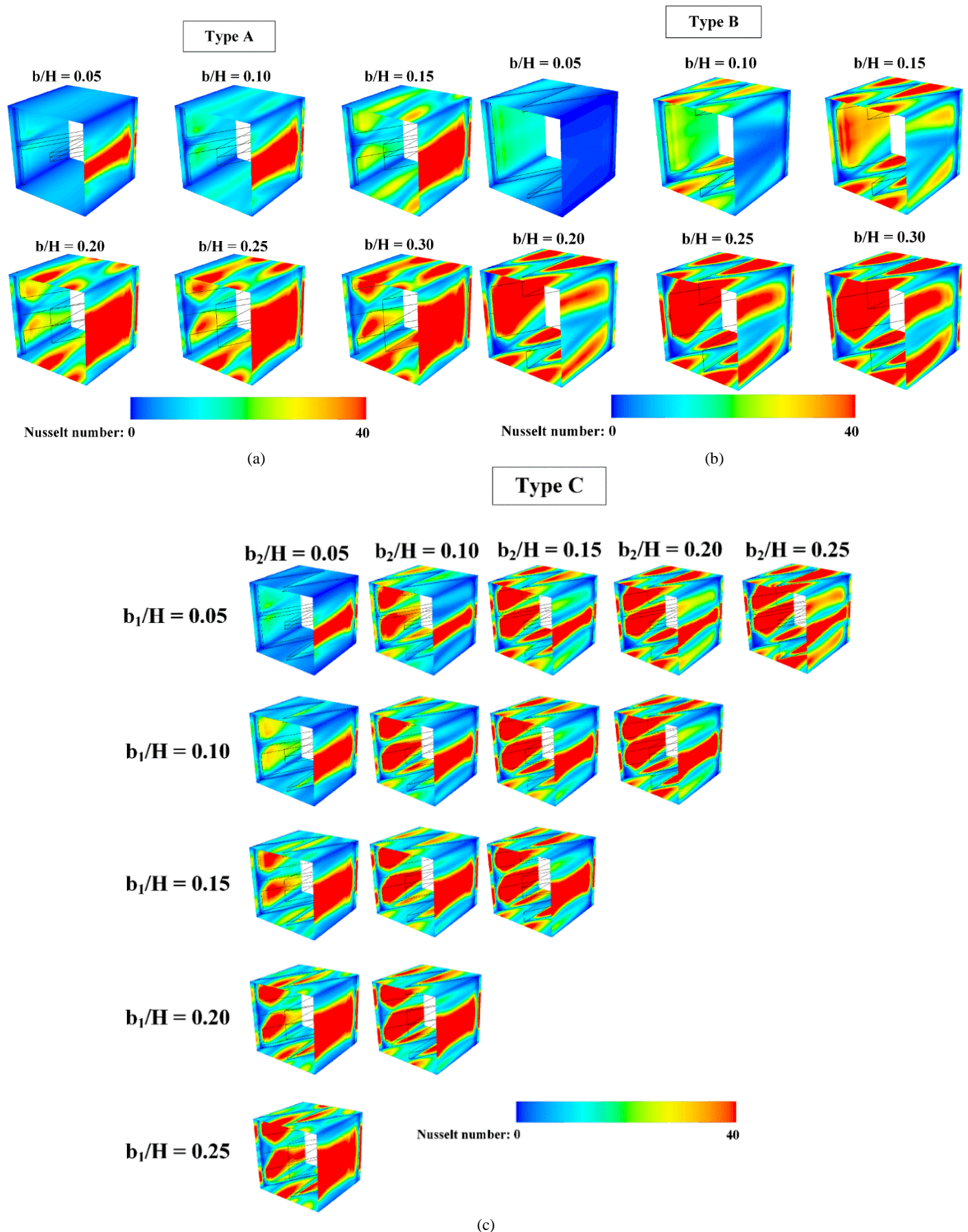
Fig. 8   Local Nusselt number contours on duct walls of the HXD equipped with (a) type A, (b) type and (c) type C DIBs at Re = 1000.

Table 1 Tested cases of the HXD equipped with type C DIB.

Case no.		Case no.		Case no.		Case no.		Case no.	
1	$b_1 = 0.05H$, $b_2 = 0.05H$	6	$b_1 = 0.10H$, $b_2 = 0.05H$	10	$b_1 = 0.15H$, $b_2 = 0.05H$	13	$b_1 = 0.20H$, $b_2 = 0.05H$	15	$b_1 = 0.25H$, $b_2 = 0.05H$
2	$b_1 = 0.05H$, $b_2 = 0.10H$	7	$b_1 = 0.10H$, $b_2 = 0.10H$	11	$b_1 = 0.15H$, $b_2 = 0.10H$	14	$b_1 = 0.20H$, $b_2 = 0.10H$		
3	$b_1 = 0.05H$, $b_2 = 0.15H$	8	$b_1 = 0.10H$, $b_2 = 0.15H$	12	$b_1 = 0.15H$, $b_2 = 0.15H$				
4	$b_1 = 0.05H$, $b_2 = 0.20H$	9	$b_1 = 0.10H$, $b_2 = 0.20H$						
5	$b_1 = 0.05H$, $b_2 = 0.25H$								

3. THEORY AND NUMERICAL METHOD

The simulated conditions can be stated as follows. The flow and heat transfer patterns in the tested HXD are steady. The tested fluid: air (300K with Pr = 0.707), is in the low velocity regime. The air is considered as incompressible fluid and has constant density and viscosity since the variation of the fluid temperature is not higher than 10ºC. As for the heat transfer mode, force convective heat transfer is measured, while heat transfer by natural convection and radiation are considered negligible. Viscous dissipation is ignored as well as body force. The no-slip wall boundary condition is applied for the tested HXD. The related equations are referred from Cengel and Ghajar, 2015.

The air velocity is presented by Reynolds number which is written in Eq. 1.

$$\text{Re} = \frac{\rho \bar{u} D_h}{\mu} \tag{1}$$

D_h is the hydraulic diameter of the square channel which is equal to H. μ and ρ are fluid viscosity and density, respectively. $\bar{u}$ is the average velocity at the inlet.

The pressure drop across the tested HXD is described by the friction factor as shown in Eq. 2.

$$f = \frac{(\Delta p / L) D_h}{1/2 \rho \bar{u}^2} \tag{2}$$

where Δp is the pressure drop across the tested section, L.

The forced convection of the tested HXD is presented by the local Nusselt and averaged Nusselt number as shown in Eqs. 3 and 6, respectively.

$$Nu_x = \frac{h_x D_h}{k} \tag{3}$$

where k is the thermal conductivity of the fluid, and h_x is the local Nusselt number which is calculated by

$$q = k \left(\frac{\partial T}{\partial n} \right) \tag{4}$$

$$h_x = \frac{q}{T_w - T_f} \tag{5}$$

Subscript; w = wall, f = local fluid and n is the local coordinate normal to the wall.

$$Nu = \frac{1}{A} \int Nu_x \partial A \tag{6}$$

The benefit of the DIB installation can be assessed by thermal enhancement factor which can be calculated with Eq. 7.

$$TEF = \frac{h}{h_0}\bigg|_{pp} = \frac{Nu}{Nu_0}\bigg|_{pp} = \frac{(Nu / Nu_0)}{(f / f_0)^{1/3}} \tag{7}$$

The Nu_0 and f_0 in Eq. 7 are the Nusselt number and the friction factor for the simple duct with no DIB, respectively.

$$Nu_0 = 2.98 \tag{8}$$

$$f = 57 / \text{Re} \tag{9}$$

The boundary conditions of the simulated model are summarized in Table 2.

Table 2 Boundary conditions of the simulated model.

Zones	Boundary conditions
Inlet-exit regime	Periodic boundary
Duct wall	Uniform temperature of 310 K
DIB	Insulator/heat flux of 0 W/m²

The simulated problem of the HXD equipped with the DIB is solved with the finite volume method using a commercial code. The governing equations in the present research are the continuity, the momentum and the energy equations. For the numerical setting, the continuity, the momentum and the energy equations are discretized by the power law scheme, the power law scheme and the QUICK scheme, respectively. In comparison, our simulated results are very close with the change of the numerical schemes (FOU, SOU, power law schemes) for the continuity and the momentum equations. The simulated solutions are set to be converged when the normalized residual data are lower than 10^{-5} for all variables, but lower than 10^{-9} for the energy equation. For the numerical test, the number of iterations is around 50,000 – 200,000.

4. NUMERICAL RESULTS

This section is divided into three parts: 1. numerical validation, 2. flow mechanism and heat transfer and 3. thermal performance assessment.

4.1 Numerical validation

For the numerical investigation, the simulated domain must be validated to assure the accuracy of the simulated results. There are two parts for the numerical validation: 1. smooth duct validation and 2. grid independence test. The smooth duct validation is done by comparing the averaged Nusselt number and the friction factor of the current smooth duct with the correlation data (Cengel and Ghajar (2015)) as depicted in Fig. 2. The Nusselt number of the present model differs from the correlation values by 0.6%, while the deviation of the friction factor is around 8%, thus validating the numerical modeling in the present study.

Figs. 3a and b present the plot comparing Nu/Nu_0 and f/f_0 with Re, respectively, at different grid cells for the HXD equipped with different DIB types. The b/H = 0.20 is selected for type A and B DIBs, while the $b_1/H = b_2/H = 0.10$ is opted for type C DIB. As shown in the figures, an

increase in the grid cells higher than 180000 cells has no impact on the Nusselt number and the friction loss in all DIB types. Therefore, the

simulated model of the HXD equipped with all DIB types is applied with the optimal number of the grid cells of around 180000.

(a)

(b)

(c)
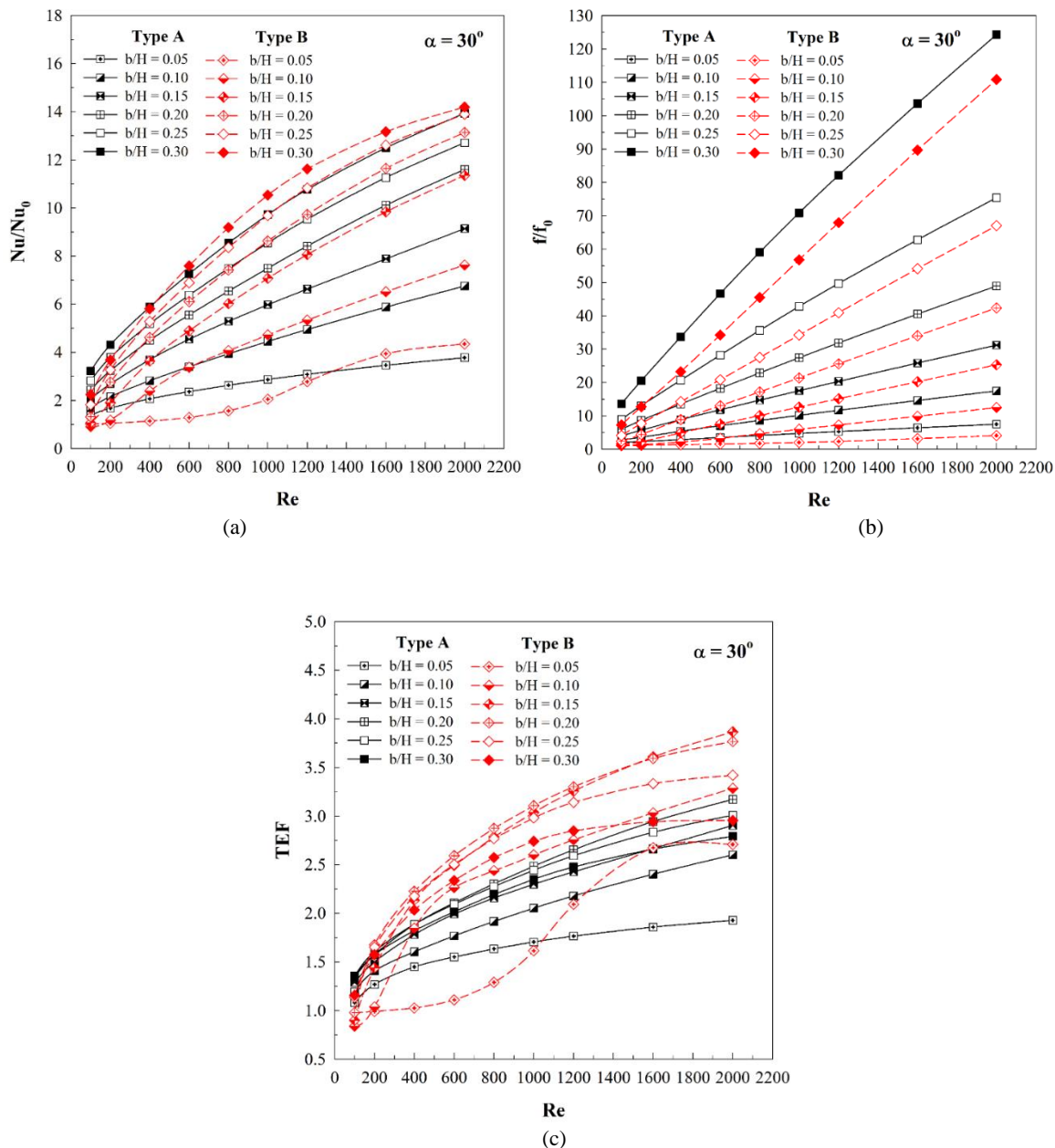
Fig. 9   Thermal performance assessment of the HXD equipped with type A and B DIBs for (a) Nu/Nu_0 vs Re, (b) f/f_0 vs Re and (c) TEF vs Re.

4.2 Flow mechanism and heat transfer

The streamlines in y-z axis (transverse plane) and longitudinal flows of the HXD installed with the DIB are presented to discuss the flow topologies. The temperature and the local Nusselt number distributions are plotted to analyze the heat transfer characteristics.

Figs. 4a, b and c present the streamlines in the cross-sectional planes of the HXD equipped with type A, B and C DIBs, respectively, of different b/H values at Re = 1000. As for type A DIB, the four major vortex centers and small vortices at the duct corners are found in all b/H cases. The symmetric flow at the upper and lower sections of the y-z plane is seen because of the symmetric DIB. Focusing at the lower pairs of the vortex flows, type A DIB in the HXD generates vortex flows in a

clockwise direction. The position of the vortex core depends on the DIB height.

As for type B DIB, the four major vortex centers and the small vortices close to the duct corners are observed for all b/H cases. The symmetric flow profile at the upper and lower sections of the cross-sectional plane is found due to the symmetric DIB. Considering at the lower pairs of the flows, type B DIB in the HXD produces the vortex flows in a counterclockwise direction for all b/H values. The vortex center location depends on the DIB height.

As for type C DIB, the eight major vortex centers are found. The symmetric flow profile at the upper and the lower parts of the transverse plane is observed because of the symmetry of the DIB shape. The vortex flows can be split into two parts.

(a)

(b)

(c)
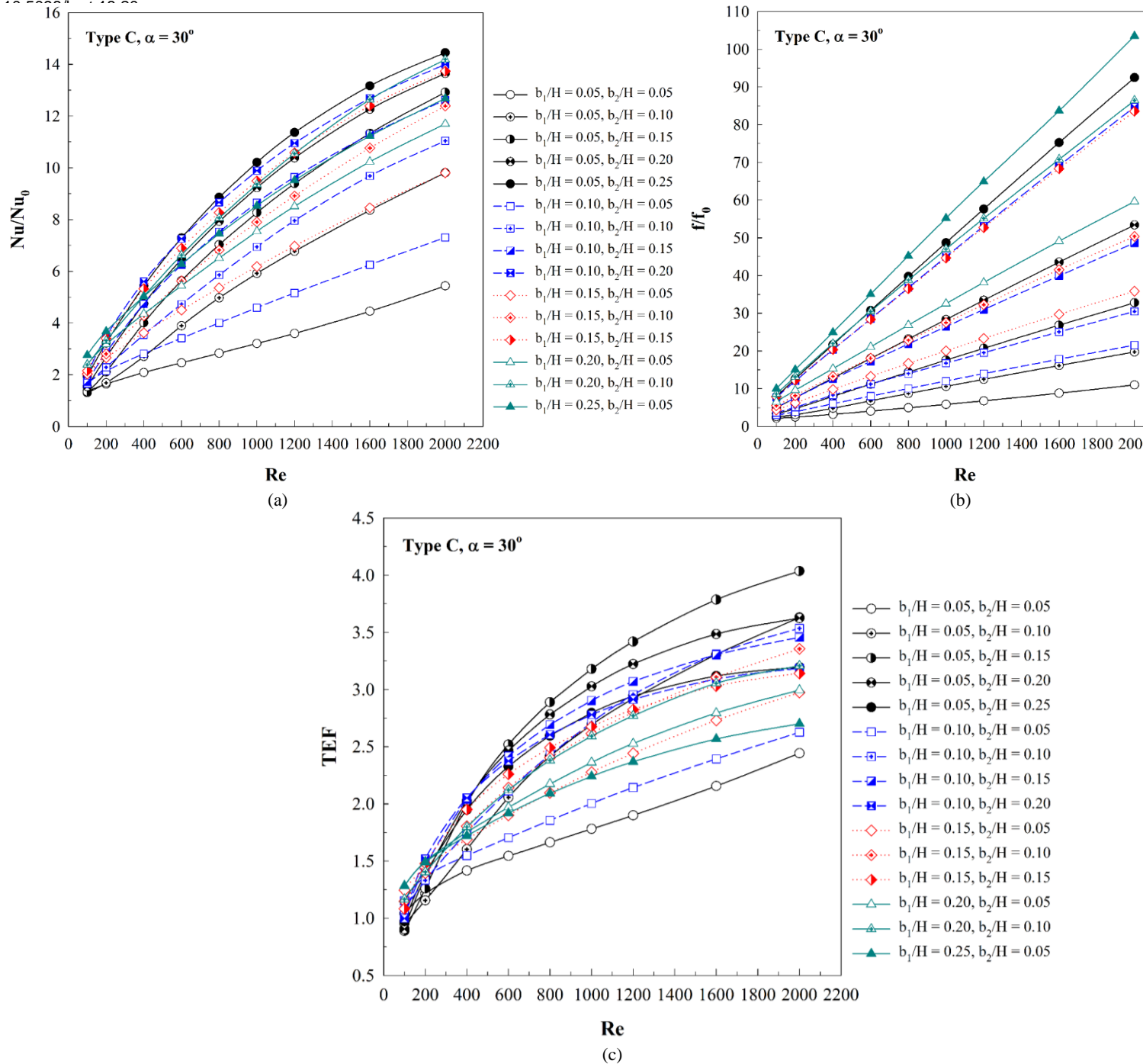
Fig. 10 Thermal performance assessment of the HXD equipped with type C DIB for (a) Nu/Nu_0 vs Re, (b) f/f_0 vs Re and (c) TEF vs Re.

11
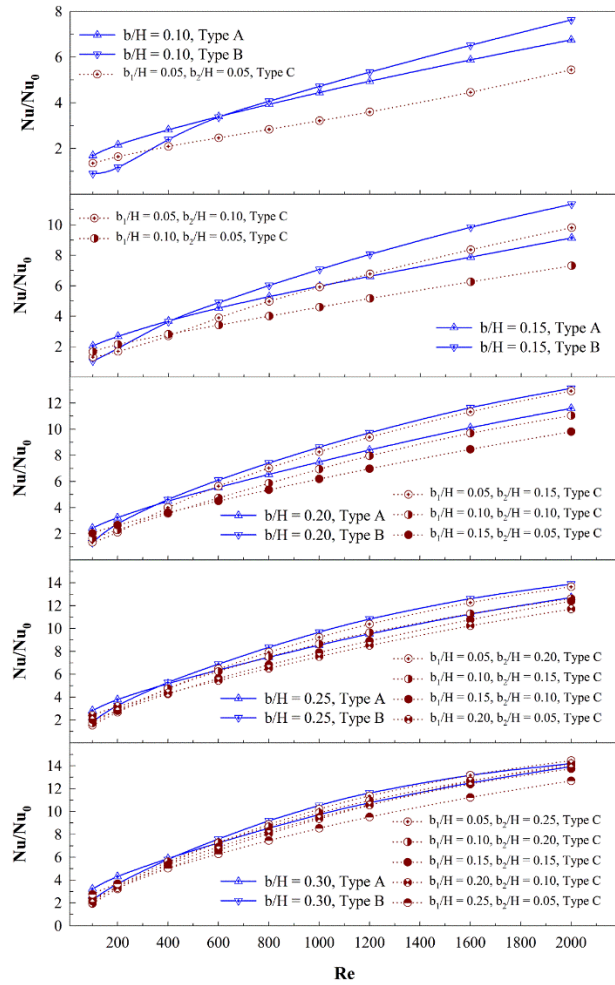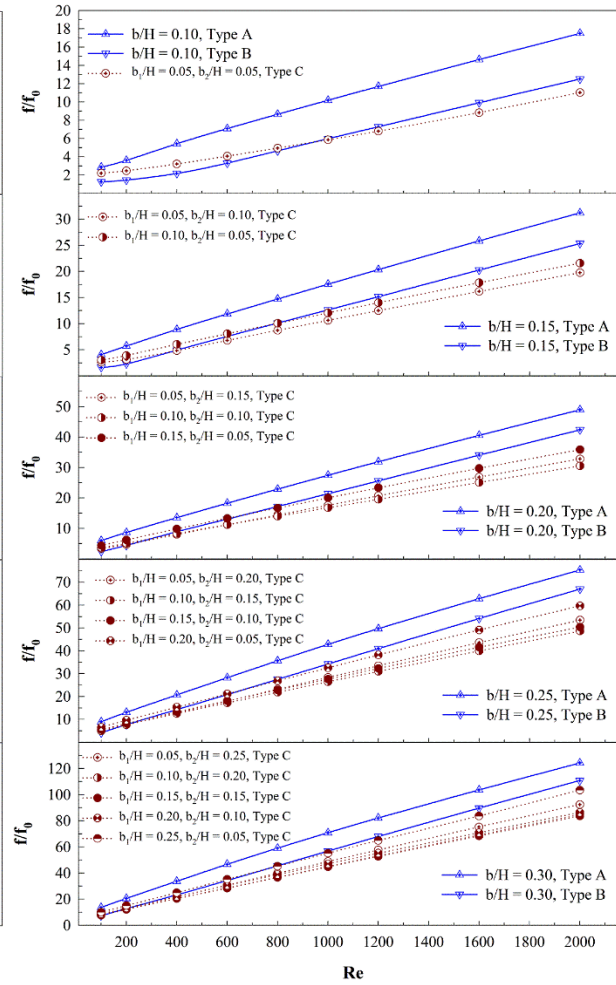
Fig. 11 Comparison in the HXD equipped with various DIB types at similar flow blockage ratios of the (a) Nu/Nu_0 vs Re, (b) f/f_0 vs Re and (c) TEF vs Re.

The vortex flows at the center of the plane (VT_1) is created by the DIB located in the middle of the HXD, while vortex flows near the upper-lower walls (VT_2) are produced by the DIB located on the upper-lo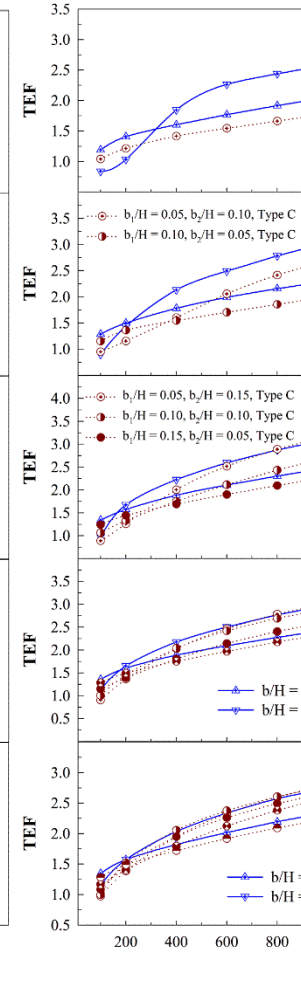wer walls. The vortex center position and the vortex flow size are varied with the DIB height. The VT_1 rotates in the clockwise direction, while the VT_2 rotates in a counterclockwise direction.

The vortex flows in the HXD play an important role in the enhancement of the heat transfer. The benefits of the vortex flows in the HXD are 1. to improve fluid blending and 2. to disturb the TBL. These two mechanisms in the HXD equipped with the DIB are the major keys for the enhanced heat transfer. An increment of the number of the vortex cores improves the air temperature distribution in the HXD. However, the power of the vortex flow may reduce with increasing the number of the vortex cores. The vortex power directly influences the enhanced heat transfer rate over the HXD.

Figs. 5a, b and c present the plots of the impinging flows of the HXD equipped with type A, B and C DIBs, respectively, at Re = 1000. The impinging flows are parts of the vortex flows in the HXD. The impinging flows directly causes the disturbance of the TBL. The impacting flows can reduce the TBL thickness which can help to increase the heat transfer coefficient. As shown in the figures, the impinging flows in the HXD are found for all DIB types. Because the flow topologies of the HXD installed with various DIB types are not in a similar pattern, the impingement positions are not in a similar position. The impinging positions may result in a higher local Nusselt number when compared with other regimes (see Fig. 7).

Figs. 6a, b and c show the temperature contours in cross-sectional planes for the HXD with type A, B and C DIBs, respectively, at Re = 1000 with various b/H cases. The variation of the temperature contours indicates the disturbance of the TBL. Normally, red contours of hot air are observed close to the duct walls, while blue layers of cold fluid are found at the core of the duct for the plain duct without DIBs. The fluid distribution is more uniform with the inserted DIB in the HXD for all DIB types.

For type A and B DIBs, the temperature contours of the b/H = 0.05 are found similarly as the temperature profiles of the smooth duct. This is because when b/H = 0.05, it generates the lowest vortex power. The fluid distribution in the HXD is found to be more uniform when increasing the b/H values because of the growth of the vortex strength. When b/H = 0.30, it performs the highest vortex strength when the b/H = 0.05 provides the reverse trend when considered at the temperature contours. The temperature profiles in the HXD with type A and B DIBs are not in a similar pattern. The TBL disturbance is obviously discovered with the increasing b/H values for both types.

For type C DIB, the disturbed TBL in the HXD is found in all cases, especially, at high flow blockage ratios. Type C DIB ($b_1/H = b_2/H = 0.05$) provides the temperature distributions nearly as the smooth duct without DIBs. The reason is that the ratio of $b_1/H = b_2/H = 0.05$ results in the lowest vortex strength. The vortex power in the HXD equipped with type C DIB increases with the increasing b_1/H and b_2/H values. Because the temperature profile of type C DIB differs from that of type A and B DIBs, the position of the disturbed TBL (or the peak position of the Nu_x) is not in a similar pattern (see the Fig. 7).

Figs. 8a, b and c present the plot of the Nu_x on the duct walls of the HXD with type A, B and C DIBs, respectively, at Re = 1000 with different b/H values. The greatest Nusselt number is presented with red layer, while the lowest Nusselt number is shown by the blue layer. The peak regime of the local Nusselt number occurs due to the disturbance of the TBL which is acted by the impinging flows. For all DIB types, an sudden increase of the Nusselt number is caused by an increase of the b/H values. For type A and B DIBs, the highest and lowest heat transfer values are observed at the DIB with the b/H of 0.30 and 0.05, respectively. For type C DIB, the lowest Nusselt number is observed when $b_1/H = b_2/H = 0.05$. The peak of the Nu_x is observed at the right sidewall for type A DIB, and is found at the left sidewall for type B DIB. For type C DIB, the peak of the Nu_x depends on the b_1 and b_2 values. The

knowledge about the position of the highest Nu_x is beneficial for some heat exchanger types which require 1 - 3 heating sides, for example.

4.3 Thermal performance assessment

There are three parts in this section: 1. enhanced heat transfer, 2. pressure loss and 3. efficiency. The enhanced heat transfer rate, pressure loss and thermal efficiency in the HXD equipped with various DIB types are described by the Nusselt number ratio (Nu/Nu_0), friction factor ratio (f/f_0) and thermal enhancement factor (TEF), respectively.

Figs. 9a, b and c show the relations of the Nu/Nu_0, f/f_0 and TEF versus the Reynolds number for the HXD equipped with type A and B DIBs, respectively. Normally, the HXD with the DIB gives better heat transfer rate than those of the plain duct with no DIB ($Nu/Nu_0 > 1$). As the Reynolds number and the DIB height increase, the Nu/Nu_0 increases. This is because the power of the vortex flow increases when rising the DIB height and the Reynolds number. The growing vortex strength directly influences the impinging flow on the duct walls that is the 1st reason for the improved heat transfer. Moreover, the growing vortex strength also impacts the fluid temperature distribution over the HXD that is the 2nd cause for the enhanced heat transfer. The friction factor of the HXD equipped with the DIB is higher than the simple duct for all tested cases ($f/f_0 > 1$). As the Reynolds number enhances, the f/f_0 rises. The f/f_0 of the HXD equipped with the DIB augments when increasing the b/H value. This is because the flow blockage directly results in the increase of the pressure drop in the HXD. For an identical flow blockage, type A DIB results in higher friction loss than type B DIB for all Reynolds numbers. The different values of the f/f_0 between type A and B DIB increase when augmenting the flow blockage ratio. The TEF of the HXD equipped with the DIB is higher than that of the simple duct for almost examples (TEF > 1). The TEF of the HXD equipped with type B DIB is higher than that of type A DIB. This means that type B DIB performs the best ratio for the heat transfer potentiality and pressure loss when compared at an identical pumping force. The best thermal potentiality of the HXD equipped with type A and B DIBs is found at the b/H of 0.15 and 0.20, respectively, at Re = 2000.

The relations of the Nu/Nu_0 vs Re, f/f_0 vs Re and TEF vs Re for the HXD equipped with type C DIB are shown in Figs. 10a, b and c, respectively. Normally, the installation of type C DIB in the HXD yields greater heat transfer coefficient and friction loss than the plain duct with no DIB in all investigated cases ($Nu/Nu_0 > 1$ and $f/f_0 > 1$). The Nusselt number for the HXD equipped with type C DIB improves when rising the Reynolds number because of the increment of the vortex power. At similar b_1/H, the Nu/Nu_0 of the HXD increases when growing the b_2/H because of the enhanced vortex power. The maximum and the minimum Nu/Nu_0 for the HXD equipped with type C DIB are found when $b_1/H = 0.05$, $b_2/H = 0.25$ and $b_1/H = b_2/H = 0.05$, respectively. As the Reynolds number and DIB height increase, the friction loss rises. The maximum f/f_0 in the HXD inserted with type C DIB is found when $b_1 = 0.25H$, $b_2 = 0.05H$, while the lowest f/f_0 is found when $b_1 = b_2 = 0.05H$. It is interesting that the b_1/H (DIB at the middle of the HXD) plays an important role to reduce the pressure drop of the HXD inserted with type C DIB. The insertion of type C DIB in the HXD provides greater TEF than that of the plain duct for almost investigated cases (TEF > 1). The best TEF for the HXD equipped with type C DIB is found when $b_1/H = 0.05$, $b_2/H = 0.15$.

Figs. 11a, b and c present the Nu/Nu_0 vs Re, f/f_0 vs Re and TEF vs Re, respectively, for the HXD equipped with various DIB types at similar total blockage ratios (b_t/H, $b_t = b$ for the type A and B DIB, $b_t = b_1+b_2$ for the type C DIB). Considering at Re = 2000, $b_t/H = 0.10$ and 0.15, the maximum Nu/Nu_0 of the HXD equipped with various DIB types is found at type B DIB. When $b_t/H = 0.20$ with Re = 2000, the highest heat transfer coefficient in the HXD is found at type B and C DIBs ($b_1/H = 0.05$, $b_2/H = 0.15$). The HXD equipped with type B and C DIBs ($b_1/H = 0.05$, $b_2/H = 0.20$) provides the best heat transfer coefficient at the total flow blockage of 0.25 when at Re = 2000. When $b_t/H = 0.30$ and Re = 2000, the values of the Nu/Nu_0 in the HXD equipped with different DIBs do not much differ, except for type C DIB when $b_1/H = 0.25$ and $b_2/H = 0.05$

where the heat transfer is the lowest. The Nusselt number of the HXD equipped with type A, B and C DIBs is 1.38 – 13.93, 1.00 – 14.19 and 1.31 – 14.45 times, respectively, higher than the simple duct with no DIB, depending on the DIB height and the Reynolds number. At similar b_t/H, it is clearly seen that the HXD equipped with type A DIB provides the highest pressure loss, while type B DIB provides higher friction loss than type C DIB for almost Reynolds numbers. This means that the DIB which is located at the middle of the HXD is significant factor for the pressure loss enhancement. The friction factor of the HXD equipped with type A, B and C DIBs is 2.09 – 124.30, 1.10 – 110.82 and 2.20 – 103.52 times, respectively, higher than that of the smooth duct without DIBs, depending on the DIB height and the Reynolds number. At the $b_t/H = 0.10$ and 0.15, the best TEF of 3.29 and 3.87, respectively, is found at the type B DIB, when considering at Re = 2000. The type C ($b_1/H = 0.05$, $b_2/H = 0.15$), type C ($b_1/H = 0.05$, $b_2/H = 0.20$) and type C ($b_1/H = 0.20$, $b_2/H = 0.10$) offer the best TEF of 4.04, 3.62 and 3.21 at the total DIB height to the duct height of 0.20, 0.25 and 0.30, respectively, at Re = 2000.

5. CONCLUSIONS

Heat transfer analysis of the HXD with various DIB styles is numerically studied. The impacts of DIB heights ($b_t/H = 0.05 – 0.30$), DIB types (A, B and C) and the Reynolds number (laminar flow, Re = 100 – 2000) on flow topologies and heat transfer in the HXD are considered. The contribution of the current research are as follows.

The flow mechanisms: vortex flows and impinging flows, are found when the HXD is equipped with DIBs. Vortex streams and impinging streams disturb the TBL that are the major reason for the augmented heat transfer. The vortex strength directly impacts the disturbance of the TBL. The vortex strength depends on the DIB height, the DIB type and the Reynolds number.

The use of type C DIB results in the best values of both heat transfer rate and thermal performance. The highest heat transfer rate of the HXD equipped with type C DIB is found when $b_1/H = 0.05$ and $b_2/H = 0.25$ which are about 14.45 times above the plain duct without DIBs. The optimal TEF of the HXD equipped with type C DIB is observed when $b_1/H = 0.05$ and $b_2/H = 0.15$ which are of about 4.04. Considering installation and maintenance, type C DIB is the most stable and simple element to install in heating/cooling systems. The DIB provides the thermal enhancement factor close to that of the V-shaped baffles (Boonloi (2014) and Boonloi and Jedsadaratanachai (2014)) and inclined baffles (Promvonge et al. (2010)).

ACKNOWLEDGEMENTS

NOMENCLATURE

b	DIB height, m
b_1	DIB height at the middle of the duct (for type C DIB), m
b_2	DIB height on the upper-lower walls of the duct (for type C DIB), m
b_t	total DIB height, m
D_h	hydraulic diameter of the tested duct, m
f	friction factor
H	square duct height, m
h	convective heat transfer coefficient, W m^{-2} K^{-1}
k	thermal conductivity, W m^{-1} K^{-1}
L	numerical model length
Nu	Nusselt number (=hD_h/k)
p	static pressure, Pa
Re	Reynolds number
T	temperature, K
$\overline{u}$	mean velocity in channel, m s^{-1}

Greek letter

α	flow attack angle, degree
ρ	density, kg m^{-3}

Subscript

0	smooth square channel
pp	pumping power

Abbreviation

DIB	dual-inclined baffle
HXD	heat exchanger duct
TBL	thermal boundary layer
TEF	thermal enhancement factor (=$(Nu/Nu_0)/(f/f_0)^{1/3}$)

REFERENCE

Ameur, H., 2019, "Effect of the Baffle Inclination on the Flow and Thermal Fields in Channel Heat Exchangers", *Results in Engineering*, **3**, September 2019, 100021.
https://doi.org/10.1016/j.rineng.2019.100021

Ameur, H., 2020, "Effect of Corrugated Baffles on the Flow and Thermal Fields in a Channel Heat Exchanger", *Journal of Applied and Computational Mechanics*, **6**, 209-218.
https://doi.org/10.22055/jacm.2019.28936.1521

Ameur, H., and Sahel, D., 2019, "Effect of Some Parameters on the Thermo-hydraulic Characteristics of a Channel Heat Exchanger with Corrugated Walls", *Journal of Mechanical and Energy Engineering*, **3**, 53-60.
https://doi.org/10.30464/jmee.2019.3.1.53.

Ameur, H., Sahel, D., and Menni, Y., 2020, "Enhancement of the Cooling of Shear-thinning Fluids in Channel Heat Exchangers by using the V-baffling Technique", *Thermal Science and Engineering Progress*, **18**, 100534.
https://doi.org/10.1016/j.tsep.2020.100534

Bahiraei, M., Mazaheri, N., and Moayedi, H., 2020, "Employing V-Shaped Ribs and Nanofluid as Two Passive Methods to Improve Second Law Characteristics of Flow within a Square Channel: A Two-phase Approach", *International Journal of Heat and Mass Transfer*, **151**, Article 119419.
https://doi.org/10.1016/j.ijheatmasstransfer.2020.119419

Bahiraei, M., Mazaheri, N., Hosseini, Y., and Moayedi, H., 2019, "A Two-phase Simulation for Analyzing Thermohydraulic Performance of Cu–water Nanofluid within a Square Channel Enhanced with 90° V-Shaped Ribs", *International Journal of Heat and Mass Transfer*, **145**, Article 118612.
https://doi.org/10.1016/j.ijheatmasstransfer.2019.118612

Barik, A.K., Mohanty, A., Senapati, J.R., and Awad, M.M., 2021, "Constructal Design of Different Ribs for Thermo-fluid Performance Enhancement of a Solar Air Heater (SAH)", *International Journal of Thermal Sciences*, **160**, Article 106655.
https://doi.org/10.1016/j.ijthermalsci.2020.106655

Boonloi, A., 2014, "Effect of Flow Attack Angle of V-Ribs Vortex Generators in a Square Duct on Flow Structure, Heat Transfer, and Performance Improvement", *Modelling and Simulation in Engineering*, **2014**, Article 985612.
https://doi.org/10.1155/2014/985612

Boonloi, A., and Jedsadaratanachai, W., 2014, "Thermal Performance Analysis and Empirical Correlations for Laminar Forced Convection over 30∘ V-Baffled Square Channel", *Advances in Mechanical Engineering*, **2014**, Article 930272.
https://doi.org/10.1155/2014/930272

Cengel, Y.A., and Ghajar, A.J., 2015, "Heat and Mass Transfer: Fundamentals & applications", Fifth edition in SI Units, McGraw-Hill Education, ISBN 978-981-4595-27-8.

Chang, S.W., Chen T.W., and Chen, Y.W., 2019, "Detailed Heat Transfer and Friction Factor Measurements for Square Channel Enhanced by Plate Insert with Inclined Baffles and Perforated Slots", *Applied Thermal Engineering*, **159**, Article 113856. https://doi.org/10.1016/j.applthermaleng.2019.113856

Jiang, W., Zhao, J., and Rao, Z., 2021, "Heat Transfer Performance Enhancement of Liquid Cold Plate Based on Mini V-shaped Rib for Battery Thermal Management", *Applied Thermal Engineering*, **189**, Article 116729. https://doi.org/10.1016/j.applthermaleng.2021.116729

Jin, D., Quan, S., Zuo, J., and Xu, S., 2019, "Numerical Investigation of Heat Transfer Enhancement in a Solar Air Heater Roughened by Multiple V-shaped Ribs", *Renewable Energy*, **134**, 78-88. https://doi.org/10.1016/j.renene.2018.11.016

Keramat, F., Dehghan, P., Mofarahi, M., and Lee, C.H., 2020, "Numerical Analysis of Natural Convection of Alumina–water Nanofluid in H-shaped Enclosure with a V-shaped Baffle", *Journal of the Taiwan Institute of Chemical Engineers*, **111**, 63-72. https://doi.org/10.1016/j.jtice.2020.04.006

Krishnaswamy, K., and Sivan, S., 2021, "Improvement in Thermal Hydraulic Performance by using Continuous V and W-Shaped Rib Turbulators in Gas Turbine Blade Cooling Application", *Case Studies in Thermal Engineering*, **24**, Article 100857. https://doi.org/10.1016/j.csite.2021.100857

Liu, C., Li, B., Ye, L., Zhu, H., Zhang, C., and Song, W., 2021, "Film Cooling Characteristics of Cross-flow Coolant Passage with Various Relative Positions of Holes and Inclined Ribs", *International Journal of Thermal Sciences*, **167**, Article 106975. https://doi.org/10.1016/j.ijthermalsci.2021.106975

Luan, N.T., and Phu, N.M., 2020, "Thermohydraulic Correlations and Exergy Analysis of a Solar Air Heater Duct with Inclined Baffles", *Case Studies in Thermal Engineering*, **21**, Article 100672. https://doi.org/10.1016/j.csite.2020.100672

Luan, N.T., and Phu, N.M., 2021, "Thermohydraulic Performance and Entropy Generation of Baffled Channel: Numerical Analysis and Optimization", *Journal of Thermophysics and Heat Transfer*. https://doi.org/10.2514/1.T6332

Menni, Y., Ameur, H., Sharifpur, M., Ahmadi, M.H., 2021, "Effects of In-line Deflectors on the Overall Performance of a Channel Heat Exchanger", *Engineering Applications of Computational Fluid Mechanics*, **15**, 512-529. https://doi.org/10.1080/19942060.2020.1815586

Ni, S., Zhao, D., Sun, Y., and E, J., 2019, "Numerical and Entropy Studies of Hydrogen-fuelled Micro-combustors with Different Geometric Shaped Ribs", *International Journal of Hydrogen Energy*, **44-14**, 7692-7705. https://doi.org/10.1016/j.ijhydene.2019.01.136

Promvonge, P., Jedsadaratanachai, W., and Kwankaomeng, S., 2010, "Numerical Study of Laminar Flow and Heat Transfer in Square Channel with 30° Inline Angled Baffle Turbulators", *Applied Thermal Engineering*, **30(11-12)**, 1292-1303. https://doi.org/10.1016/j.applthermaleng.2010.02.014

Rathor, Y., and Aharwal, K.R., 2020, "Heat Transfer Enhancement Due to a Staggered Element Using Liquid Crystal Thermography in an Inclined Discrete Rib Roughened Solar Air Heater", *International Communications in Heat and Mass Transfer*, **118**, Article 104839. https://doi.org/10.1016/j.icheatmasstransfer.2020.104839

Sivakandhan, C., Arjunan, T.V., and Matheswaran, M.M., 2020, "Thermohydraulic Performance Enhancement of a New Hybrid Duct Solar Air Heater with Inclined Rib Roughness", *Renewable Energy*, **147-11**, 2345-2357. https://doi.org/10.1016/j.renene.2019.10.007

Srivastava, A., Chhaparwal, G.K., and Sharma, R.K., 2020, "Numerical and Experimental Investigation of Different Rib Roughness in a Solar Air Heater", *Thermal Science and Engineering Progress*, **19**, Article 100576. https://doi.org/10.1016/j.tsep.2020.100576

Thao, P.B., Truyen, D.C., and Phu, N.M., 2021. "CFD Analysis and Taguchi-Based Optimization of the Thermohydraulic Performance of a Solar Air Heater Duct Baffled on a Back Plate", *Applied Sciences,* **11**, 4645. https://doi.org/10.3390/app11104645

Yuan, N., Bi, D., Zhai, Y., Jin, Y., Li, Z., and Wang, H., 2020, "Flow and Heat Transfer Performance of Supercritical Pressure Carbon Dioxide in Pipes with Discrete Double Inclined Ribs", *International Journal of Heat and Mass Transfer*, **149**, Article 119175. https://doi.org/10.1016/j.ijheatmasstransfer.2019.119175

Zhao, Z., Luo, L., Qiu, D., Wang, Z., and Sundén, B., 2021, "On the Solar Air Heater Thermal Enhancement and Flow Topology Using Differently Shaped Ribs Combined with Delta-winglet Vortex Generators", *Energy*, **224**, Article 119944. https://doi.org/10.1016/j.energy.2021.119944

Zheng, D., Wang, X., and Yuan, Q., 2019, "Numerical Investigation on the Flow and Heat Transfer Characteristics in a Rectangular Channel with V-shaped Slit Ribs", *Infrared Physics & Technology*, **101**, 56-67. https://doi.org/10.1016/j.infrared.2019.06.004